Deformation Induced Phase Transformation of 304L Stainless Steel and its Structural Characterization

A THESIS SUBMITTED IN PARTIAL FULFILMENTS OF REQUIREMENTS FOR THE AWARD OF THE DEGREE OF

Bachelor of Technology

Submitted to

NATIONAL INSTITUTE OF TECHNOLOGY, ROURKELA

By

P. Sampark

109MM0128

Goutam Kumar Majhi

109MM0447

DEPARTMENT OF METALLURGICAL & MATERIALS ENGINEERING

NATIONAL INSTITUTE OF TECHNOLOGY

ROURKELA – 769008

INDIA

2013

Deformation Induced Phase Transformation of 304L Stainless Steel and its Structural Characterization

A THESIS SUBMITTED IN PARTIAL FULFILMENTS OF REQUIREMENTS FOR THE AWARD OF THE DEGREE OF

Bachelor of Technology

Submitted to

NATIONAL INSTITUTE OF TECHNOLOGY, ROURKELA

By

P. Sampark

109MM0128

Goutam Kumar Majhi

109MM0447

Under the Guidance of **Dr. K. Dutta**

DEPARTMENT OF METALLURGICAL & MATERIALS ENGINEERING

NATIONAL INSTITUTE OF TECHNOLOGY

ROURKELA – 769008

INDIA

2013

NATIONAL INSTITUTE OF TECHNOLOGY ROURKELA

CERTIFICATE

This is to certify that the thesis entitled ***"DEFORMATION INDUCED PHASE TRANSFORMATION OF 304L STAINLESS STEEL AND ITS STRUCTRAL CHACTERIZATION"*** *submitted by* ***P. Sampark*** *(109MM0128) and* ***Goutam Kumar Majhi*** *(109MM0447) in partial fulfillment of the requirements for the award of the degree of* ***BACHELOR OF TECHNOLOGY*** *in* ***Metallurgical and Materials Engineering*** *at the* ***National Institute of Technology, Rourkela*** *is an original work carried out by them under my supervision and guidance.*

The matter embodied in the thesis has not been submitted to any other University/ Institute for the award of any degree.

Dr. Krishna Dutta
Dept. of Metallurgical and Materials Engineering,
National Institute of Technology Rourkela – 769008

Date: 08/05/2013

ACKNOWLEDGEMENTS

We avail this opportunity to express our deep sense of gratitude to **Dr. Krishna Dutta**, our guide and supervisor for his invaluable guidance, motivation and constant inspiration. He has always bestowed parental care upon us and evinced keen interest in solving our problems. An erudite teacher, a magnificent person and a strict disciplinarian, we consider ourselves fortunate to have worked under his supervision.

We express our sincere gratitude to **Prof. B. C. Ray**, Head of the Department, Metallurgical and Materials Engineering, NIT Rourkela for giving us an opportunity to work on this project and allowing us access to valuable facilities in the department.

We are extremely thankful to **Prof S. Sarkar** and **Prof. A. Basu**, Project Coordinators, for their help and advice during the course of this work.

We are also grateful to **Mr. Shyamu Hembram**, Metallurgical & Materials Engineering Department, NIT Rourkela, for providing valuable assistance and insight during the experimental process.

We shall fail in our duty if we don't express our heartful gratitude to our parents and friends who have remained to be a constant source of inspiration throughout the period of our stay in NIT Rourkela.

Last but not the least, despite all our efforts, if any error has crept by us into this project, we beg excuse to the readers for the same.

P. Sampark(109MM0128)

Goutam Kumar Majhi (109MM0447)

Date: 08/05/2013

Dept. of Metallurgical and Materials Engineering,
National Institute of Technology, Rourkela-769008

CONTENTS

List of figures

List of tables

Abstract

This report aims to examine deformation induced phase transformation in 304L stainless steel up on compressive loading at room temperature of 300K. For this, compression tests were carried out using specimens of varying length to diameter ratios. To avoid effects of any friction, teflon tapes were use at the specimen platen interfaces. The results indicate that homogenous deformation takes place up to 15% of total compressive engineering strain. X-ray diffraction and scanning electron microscopic studies indicate that metastable austenite transforms to martensite due to compressive loading. "The volume fraction of martensite increases with increase in percentage of deformation." Post deformation hardness also increases monotonically. Nature of homogenous deformation also gets reduced due to prevailing friction at the interfaces. In the course of the study, the amounts of particular phase fractions have also been calculated from the integrated intensity of XRD results. The results are then correlated with the extent of deformation in the respective samples and the behavior is compared as-against tensile loading conditions.

Keywords: 304L Stainless steel, Compressive deformation, Deformation induced martensite, X-ray diffraction, Volume fraction.

Chapter 1

Introduction

Austenitic stainless steels find a wide range of applications in numerous engineering sectors *viz.* nuclear power plants, gas turbine components, underwater pipelines etc. **[1]**. This is due to the metallurgical advantages they offer. They can be made soft enough (i.e., with a yield strength about 200 MPa) to be easily formed by the same tools that work with carbon steel, but they can also be made incredibly strong by cold working, up to yield strengths of over 2000 MPa. The austenitic (fcc) structure of this group of steels is very tough and ductile down to absolute zero. Moreover, these steels also do not lose their strength at elevated temperatures as rapidly as ferritic (bcc, body-centered cubic) iron base alloys. The least corrosion-resistant versions can withstand the normal corrosive attack of the everyday environment that people experience, while the most corrosion-resistant grades can even withstand boiling seawater. Above all, it can be said that austenitic stainless steels are user friendly metal alloys with life-cycle cost of fully manufactured products lower than many other materials **[2]**.

Needless to mention that these steels face various types of applied stresses in their service that may be cyclic, static tensile or static compressive in nature. It is well-known that austenitic stainless steel is metastable upon deformation by which austenite transforms to martensite. The plastic deformation results in the transformation of parent austenite (γ) to martensite of hexagonal close-packed (ε) and/or body-centered cubic (α') crystal structures **[3,4]**. Such a transformation to martensite during plastic deformation is advantageous as it imparts a good combination of strength and toughness to austenitic stainless steels.

Therefore for a better understanding of the plastic deformation behavior of austenitic stainless steels, it is a-priori to have the knowledge on the martensitic transformation characteristics. Although quite an exhaustive number of research papers and journals exist for behavior under tensile testing conditions, but as per the knowledge of the current investigators no report is

available for martensitic transformation and their quantification under compressive loading conditions. This investigation aims to examine compressive deformation behavior of 304L stainless steel in samples with varying L/D ratios followed by examination of phase transformation of the steel and estimation of its volume fraction of the transformed phases.

1.1 Objectives

The major objectives and the pertinent work-plan to fulfill these can be broadly summarized as:

I. To characterize the microstructure of the investigated steel and to perform its chemical analysis.

II. To study uniaxial compressive deformation behavior of 304L stainless steel and to compare the results with tensile tests that has been performed at varying starin rates.

III. To examine possible alterations in the microstructure of the investigated steel due to compressive deformation and to compare the hardness values before and after compression tests.

The thesis has been structured into five chapters. The significance of the problem and the motivation behind this investigation are briefed in **Chapter-1**. Some pertinent literature background related to the current investigation has been presented in **Chapter-2**.**Chapter-3** consists of the experimental procedure adopted on the investigated materials.**Chapter-4** includes the results and discussion corresponding to the objectives mentioned. An overview of the conclusions derived from this investigation has been summarized briefly in **Chapter-5** together with some proposed future work related to this area. All references cited throughout the dissertation have been compiled at the end of **Chapter-5**.

Chapter 2

Literature review

2.1. Stainless Steels

In metallurgy, stainless steel, also known as inox steel **[5]**, is a steel alloy with a minimum of 10.5% to 11% chromium content by mass. Stainless steel does not readily corrode, rust or stain with water as ordinary steel does, but despite the name it is not fully stain-proof, most notably under low oxygen, high salinity, or poor circulation environments.

Stainless steel differs from carbon steel by the amount of chromium present. Unprotected carbon steel rusts readily when exposed to air and moisture. This iron oxide film (the rust) is active and accelerates corrosion by forming more iron oxide, and due to the greater volume of the iron oxide this tends to flake and fall away. Stainless steels contain sufficient chromium to form a passive film of chromium oxide, which prevents further surface corrosion and blocks corrosion from spreading into the metal's internal structure, and due to the similar size of the steel and oxide ions they bond very strongly and remain attached to the surface **[6]**.

The stainless steel family tree has several branches, which may be differentiated in a variety of ways e.g. in terms of their areas of application, by the alloying elements used in their production, or, perhaps the most accurate way, by the metallurgical phases present in their microscopic structures:

i. Ferritic
ii. Martensitic (including precipitation hardening steels)
iii. Austenitic
iv. Duplex steels, consisting of mixture of ferrite and austenite

Of these, austenitic steels make up over 70% of total stainless steel production **[7]**.

2.1.1. Austenitic stainless steel

The austenitic steels are characterised by very good corrosion resistance, very good toughness and very good weldability; they are also the most common stainless steels.

Resistance to general corrosion, pitting and crevice corrosion generally increases with increasing levels of chromium and molybdenum, while high levels of nickel and molybdenum are required to increase resistance to stress corrosion cracking. Resistance to pitting and crevice corrosion thus increases in the order: AISI 304 / 304L - 316 / 316L -317L - '904L' - '254 SMO' — '654 SMO'. The low carbon grades exhibit good resistance to intergranular corrosion and consequently the higher alloyed steels are only available with low carbon contents. The stabilised steels (AISI 321, 347 and 316Ti) and the nitrogen-alloyed steels (304LN and 316LN) have roughly the same corrosion properties in most environments as the equivalent low-carbon grades: 304L and 316L respectively. There are however, exceptions to this rule so it should be treated with some caution. Austenitic steels are generally susceptible to stress corrosion cracking; only the highly alloyed steels '904L', '254 SMO' and '654 SMO' exhibit good resistance to this type of corrosion. An increased level of chromium and silicon, in combination with additions of rare earth metals (cerium), gives an increased resistance to high temperature corrosion, which is exploited in '153 MA', '253MA' and '353MA' **[8]**.

The austenitic stainless steels are used in almost all types of applications and industries. Typical areas of use include piping systems, heat exchangers, tanks and process vessels for the food, chemical, pharmaceutical, pulp and paper and other process industries. Non-molybdenum alloyed grades, e.g. 304 and 304L, are normally not used in chloride-containing media but are often used where demands are placed on cleanliness or in applications in which equipment must not contaminate the product. The molybdenum-alloyed steels are used in chloridecontaining

environment with the higher alloyed steels, '904L', '254 SMO' and '654 SMO', being chosen for higher chloride contents and temperatures. Grades such as '254 SMO' and '654 SMO' are used to handle sea water at moderate or elevated temperatures. Applications include heat exchangers, piping, tanks, process vessels, etc. within the offshore, power, chemical and pulp & paper industries **[8]**.

The low alloyed grades, especially 304, 304LN and 304N but also 316LN, are used in equipment for cryogenic applications. Examples are tanks, heaters, evaporator and other equipment for handling of condensed gases such as liquid nitrogen.

Another use is in high temperature applications or equipment designed for elevated temperature service. In these cases both the good creep resistance and the good oxidation resistance of the austenitic steels are exploited. High carbon grades (AISI 304H) and stabilised steels (AISI 321, 347 and 316Ti) or nitrogen-alloyed steels (AISI 304LN and 316LN) are used at elevated and moderately high temperatures depending on the service temperature and environment. At higher temperatures (above about 750 ^{o}C) special high temperature or heat resistant grades are needed, such as 310, '153 MA', '253MA' and '353MA'. Typical applications for the heat resistant steels are furnace components, muffles, crucibles, hoods, recuperators, cyclones and conveyor belts working at high 38 temperatures. The high alloyed heat resistant grades, such as '353MA', are used in aggressive high temperature environments, such as those encountered in waste incineration **[6]**.

Finally it is worth mentioning that austenitic stainless steels are often used in applications requiring non-magnetic materials since they are the only non-magnetic steels.

2.1.1.1. Austenitic group

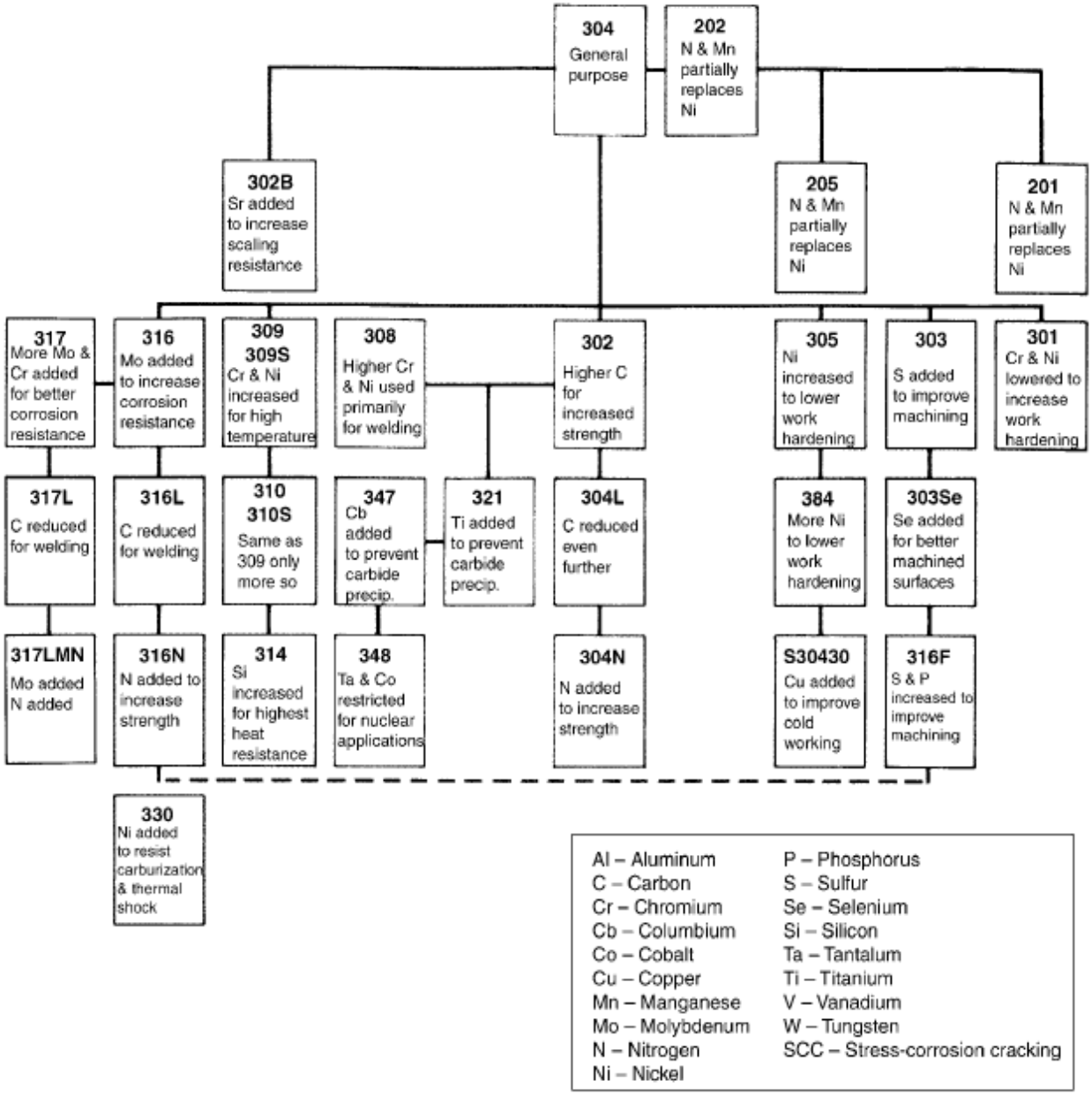

Fig 1: The austenitic stainless family. Source **[2]**

- ✓ **Straight Grades**

The straight grades of austenitic stainless steel contain a maximum of .08% carbon. There is a misconception that straight grades contain a minimum of 0.03% carbon, but the spec does not require this. As long as the material meets the physical requirements of straight grade, there is no minimum carbon requirement **[9]**.

- ✓ **"L" Grades**

The "L" grades are used to provide extra corrosion resistance after welding. The letter "L" after a stainless steel type indicates low carbon (as in 304L). The carbon is kept to 0.03% or under to avoid carbide precipitation. Carbon in steel when heated to temperatures in what is called the critical range ($800\ ^0$ F to $1600\ ^0$ F) precipitates out, combines with the chromium and gathers on the grain boundaries. This deprives the steel of the chromium in solution and promotes corrosion adjacent to the grain boundaries. By controlling the amount of carbon, this is minimized. For weldability, the "L" grades are used. But all stainless steels are not produced as "L" grades. This is because the "L" grades are more expensive. In addition, carbon, at high temperatures imparts great physical strength **[9]**.

- ✓ **"H" Grades**

The "H" grades contain a minimum of 0.04% carbon and a maximum of 0.10% carbon and are designated by the letter "H" after the alloy. "H" grades are primarily used when the material will be used at extreme temperatures as the higher carbon helps the material retain strength at extreme temperatures.

In "solution annealing", only the carbides which may have precipitated (or moved) to the grain boundaries are put back into solution (dispersed) into the matrix of the metal by the annealing

process. “H” grades are used where annealing after welding is impractical, such as in the field where pipe and fittings are being welded **[9]**.

- ✓ **Type 304**

The most common of austenitic grades, containing approximately 18% chromium and 8% nickel. It is used for chemical processing equipment, for food, dairy, and beverage industries, for heat exchangers, and for the milder chemicals **[9]**.

- ✓ **Type 316**

It contains 16% to 18% chromium and 11% to 14% nickel. It also has molybdenum added to the nickel and chrome of the 304. The molybdenum is used to control pit type attack.

Type 316 is used in chemical processing, the pulp and paper industry, for food and beverage processing and dispensing and in the more corrosive environments. The molybdenum must be a minimum of 2% **[9]**.

- ✓ **Type 317**

It contains a higher percentage of molybdenum than 316 for highly corrosive environments. It must have a minimum of 3% molybdenum. It is often used in stacks which contain scrubbers.

- ✓ **Type 317L**

Here, the maximum carbon content is restricted to 0.030% max. and silicon to 0.75% max. for extra corrosion resistance.

- ✓ **Type 317LM**

It requires a minimum molybdenum content of about 4%.

- ✓ **Type 317LMN**

It requires a minimum molybdenum content of 4% min. and nitrogen of 0.15%.

- ✓ **Type 321, Type 347**

These types have been developed for corrosive resistance for repeated intermittent exposure to temperature above 800 ^{0} F. Type 321 is made by the addition of titanium and Type 347 is made by the addition of tantalum/columbium. These grades are primarily used in the aircraft industry **[9]**.

2.2. Deformation induced martensite

Low temperature plastic deformation of type 304 austenitic stainless steel results in the transformation of parent austenite (γ) to martensite of hexagonal close-packed (ε) and/or body-centered cubic (α′) crystal structures **[10,11,12]**.

When the chemical free energy of austenite is equal to that of martensite, they are in thermodynamically in equlibrium at T_0 as shown in the figure below. It is however, necessary to undercool below the M_s temperature to start the martensitic transformation due to existence of non-chemical energy barriers such as interfacial and elastic energy.The critical driving force is therefore the minimum free energy ΔG_{crit} required for initialising martensitic transformation, which in turn corresponds to the chemical free energy difference ΔG_{ch} between the undeformed austenite and martensite phase at M_s temperature when there are no additional enegies available **[13,14]**. Martensitic transformation is also known to be triggered abobe M_s and below M_d temperature if an additional energy is supplied in the form of strain energy during inelastic deformation.

M_d (°C) = 551 – 462(%C + %N) – 9.2(%Si) – 8.1(%Mn) – 13.7(%Cr) – 29(%Ni + %Cu) – 18.5(%Mo) – 68(%Nb).

This is the temperature at which 50% of the austenite transforms to martensite **[2]**.

a)

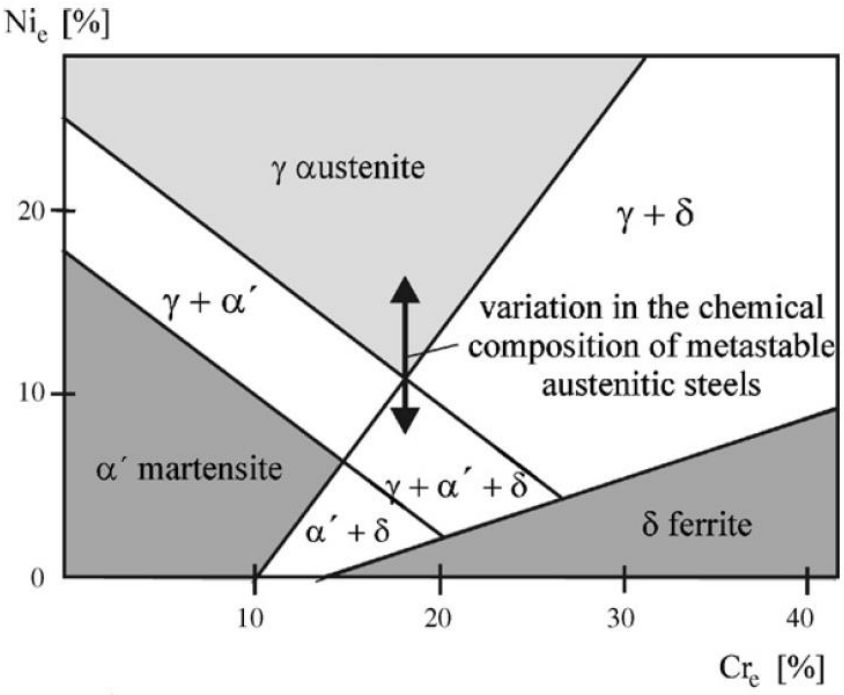

b)

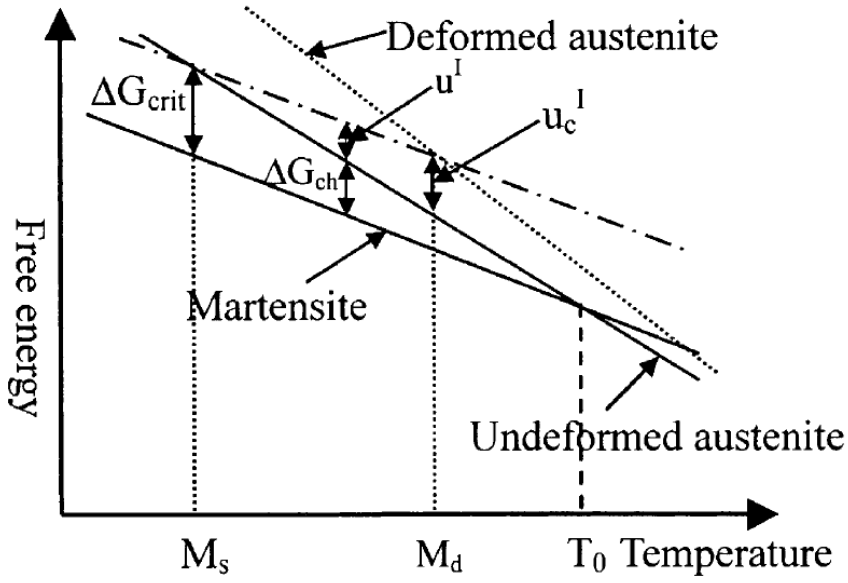

Fig 2: Schematic representation of (a) the Schaeffler diagram and (b) the contribution of the mechanical deformation energy to the driving force for austenite-to-martensite transf **[15]**.

The internal strain energy u^I, viewed here as an additional driving force for transformation, develops as a consequence of dislocation pile-ups at strong barriers such as grain boundaries during the inelastic deformation **[13,14]**. The required internal strain energy for deformation induced martensitic transformation can therefore be described as $u^I = \Delta G_{cric} - \Delta G_{ch}$.

From the engineering point of view, the deformation temperature and the deformation degree are the most important parameters determining the process of deformation-induced martensite formation in metastable austenitic steels.

Krupp et al.[16] has tried to relate the martensite volume fraction and the temperature increase during cold rolling of AISI301 coupons from an initial thickness of 2mm to an end thickness of 0.8 mm..**Fig 3** reveals that due to the temperature effect the martensite volume fraction was by a factor of almost two higher for multi-step rolling than for two-step rolling.

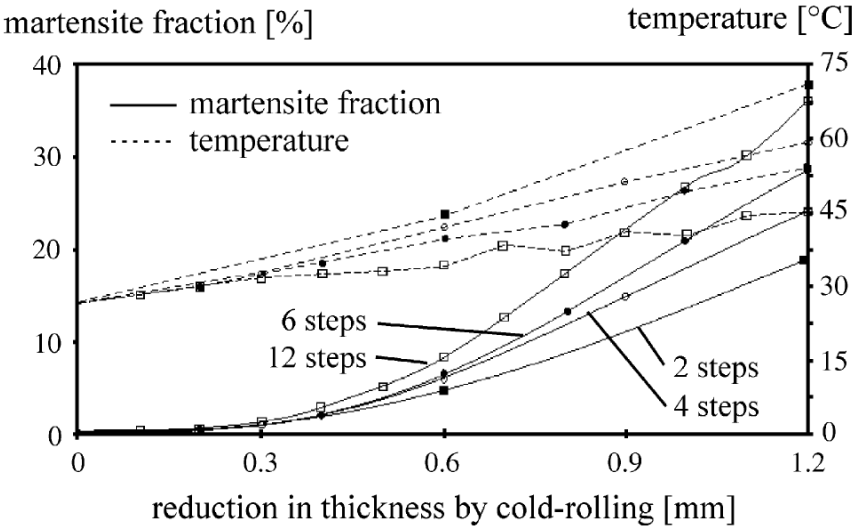

Fig 3: Development of the temperature and the martensite volume fraction during cold-rolling of AISI301 austenitic stainless steel **[16]**.

Fig. 4 shows cyclic deformation curves for three different temperatures between $T = -100$ and room temperature. In the case of the relatively high carbon concentration of $c_C = 0.09\%$, room temperature fatigue at $\Delta\varepsilon/2 = 0.5$ does not cause any pronounced strengthening. This is completely different at sub-zero temperatures: During the initial stage, strong cyclic strengthening in combination with massive deformation-induced martensite formation was observed, followed by a saturation stage. Since the higher martensite volume fraction coincides with a complete change in the stress/stain response, the plastic strain amplitude within the saturation stage is small and falls below the critical threshold value.

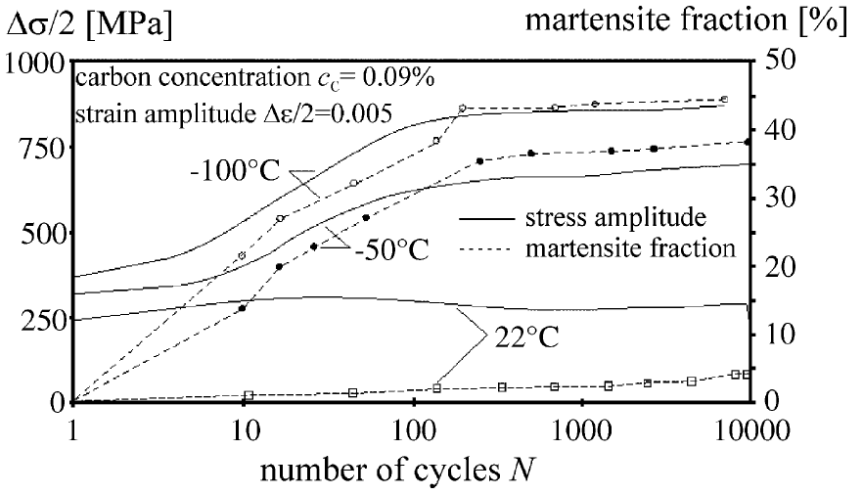

Fig 4: Cyclic deformation curves for fully reversed fatigue of AISI301 austenitic stainless steel at three different temperatures **[17]**.

The cyclic martensite formation curves for materials showing deformation-induced phase transformation are generally of sigmoidal shape. It should be noted that not only a critical threshold value of the plastic-strain amplitude but also a certain amount of accumulated plastic strain needs to be exceeded to initiate the deformation induced martensite formation. This is

manifested by the incubation time, which can be observed in general during cyclic deformation of metastable austenitic steels (see **Fig. 5)**.

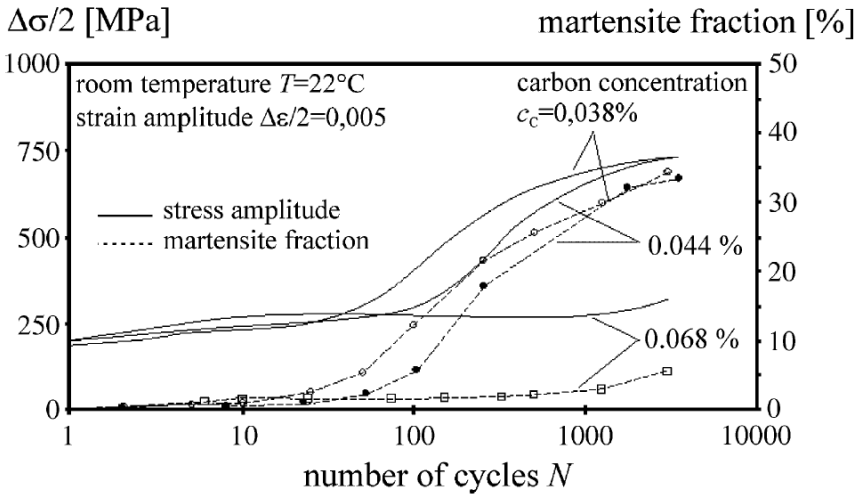

Fig 5: Cyclic deformation curves for fully reversed fatigue of AISI301 austenitic stainless steel with three different carbon concentrations **[17]**.

Dutta et al. [18] has examined the evolution of ratcheting strain in AISI 304LN stainless steel with respect to the possible variation of substructure and transformation of austenite to martensite, through stress-controlled uniaxial ratcheting tests, at various combinations of mean stress and stress amplitude.

A typical TEM bright field image along with the corresponding selected area diffraction pattern is shown in **Fig. 6** to provide evidence for the formation of martensite during ratcheting of this steel. X-ray diffraction analyses show that both ε-martensite (hcp) and α′-martensite (bcc) peaks are present in the diffraction pattern **(Fig 7).**

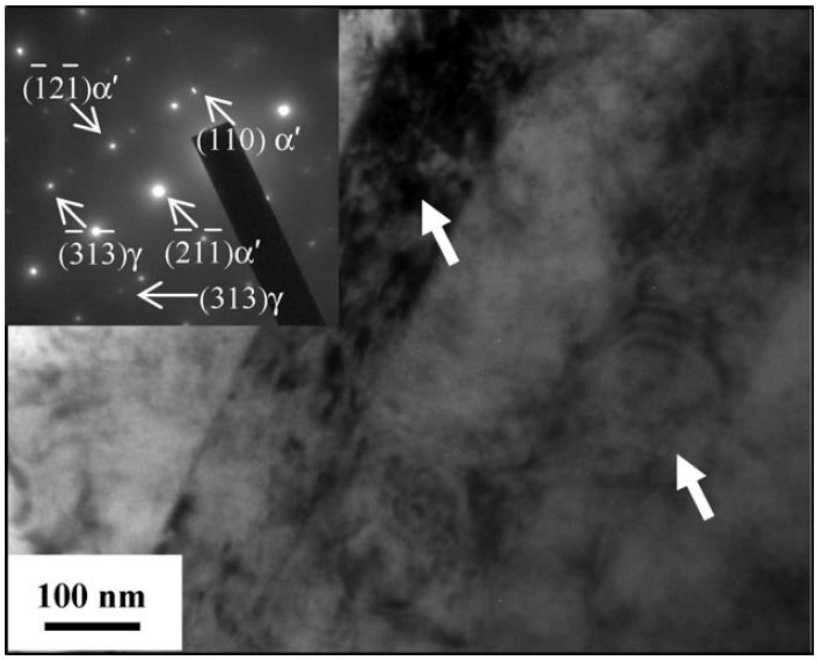

Fig 6: Formation of α′-martensite (bcc) (directed by arrow markings) with zone axis of [−113] in γ-austenite (fcc) with zone axis of [−2 3 3] **[18]**.

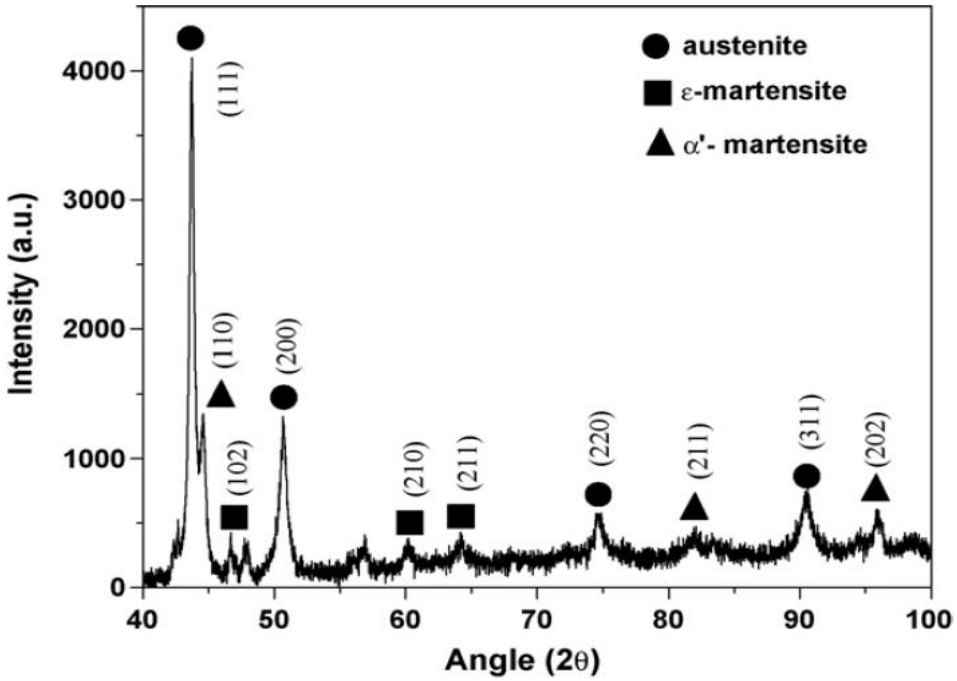

Fig. 7: X-ray diffraction pattern showing formation of ε- and α′-martensite **[18]**.

Das et al. [20] has investigated the evolution of deformation induced marrtensite during tensile deformation of 304 LN stainless steel at various strain rates. It is interesting to note that at all strain rates, the nature of variation of volume fraction of martensite with true strain is similar.

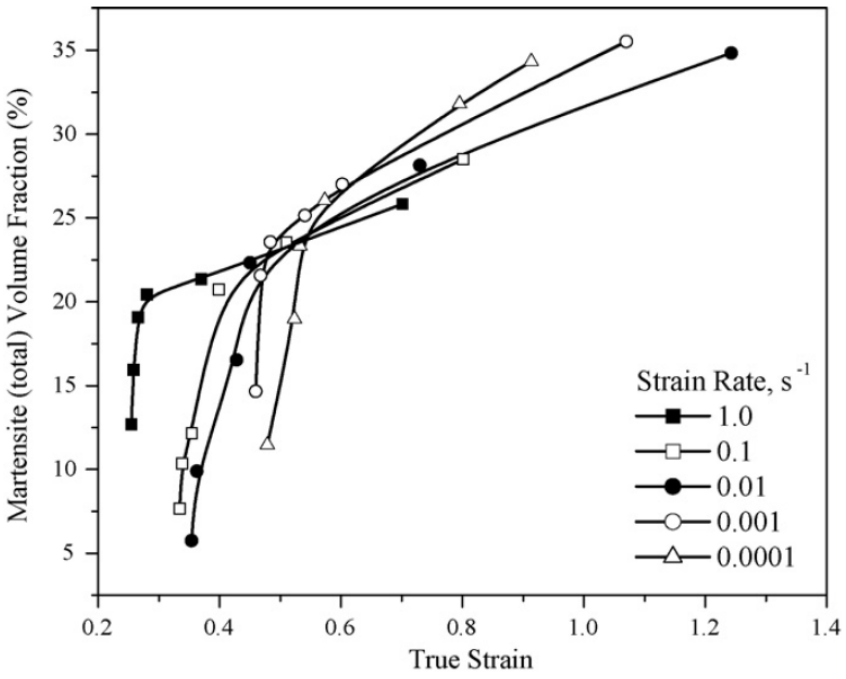

Fig 8: Volume fraction of deformation induced martensite with true strain in 304LN stainless steel at various strain rates **[20]**.

De et al. [3] has shown influence of grain size dependence of martensite transformation in 304 austenitic stainless steel. A modest grain size effect on martensite transformation is observed, but only at higher strains. A greater volume fraction of α′-martensite is obtained in the fine grain material for a given strain level. Also, ε-martensite formation in the coarse-grain sample is extended to higher strains.

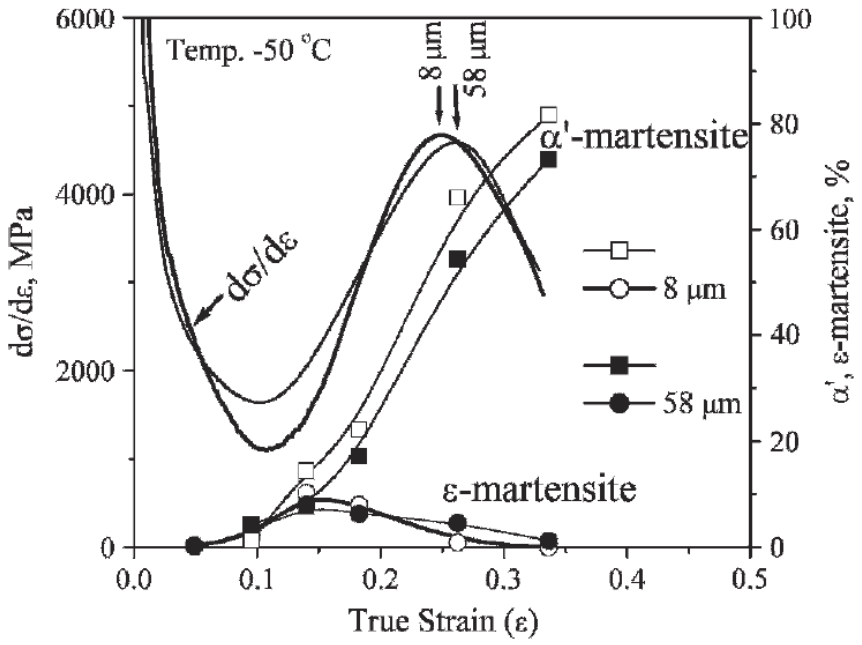

Fig 9 : Summary of grain size influence on the strain hardening behavior and phase fractions in the type 304 stainless steel **[3]**.

Therefore, the extent of transformation is dependent on the deformation temperature, strain, and grain size. **[10,11,12]** Earlier research on type 304 stainless steel postulated that ε-martensite is an intermediate or transient phase during $\gamma \rightarrow \alpha'$ transformation with an orientation relationship with parent austenite as $(111)\gamma//(001)\varepsilon$, and that the plates of bcc martensite having $\{225\}\gamma$ habit plane nucleate from the hcp structures. **[11,21,22] .** These observations are rationalized considering the low stacking fault energy of type 304 steels. More recent observations with high-resolution electron microscopy have demonstrated that both forms of martensite can be produced independently during deformation—i.e., the presence of ε-martensite is not a prerequisite to α′-martensite formation **[23,24]**. While ε-martensite forms from overlapping stacking faults on every other $\{111\}\gamma$ plane by the passage of a/6 $<112>\gamma$ Shockley partial dislocations, α′ martensite is reported to form at intersections between two shear bands. The shear bands can be

ε martensite, mechanical twins, dense stacking faults, or twin boundaries. However, during plastic deformation, the ε-martensite eventually transforms to a′-martensite at higher strains, so that at larger strains only α′-martensite is observed in 304 stainless steels. A possible mechanism proposed for this transformation is the shifting of faulted planes in the hcp phase by a second a/12 <112>γ shear resulting in a bcc martensite structure.

The transformation sequence and the mechanism significantly influence the stress-strain behavior of type 304 austenitic steel, and distinct stages are observed in flow behavior corresponding to inherent microstructural changes as shown in **Fig 10**.

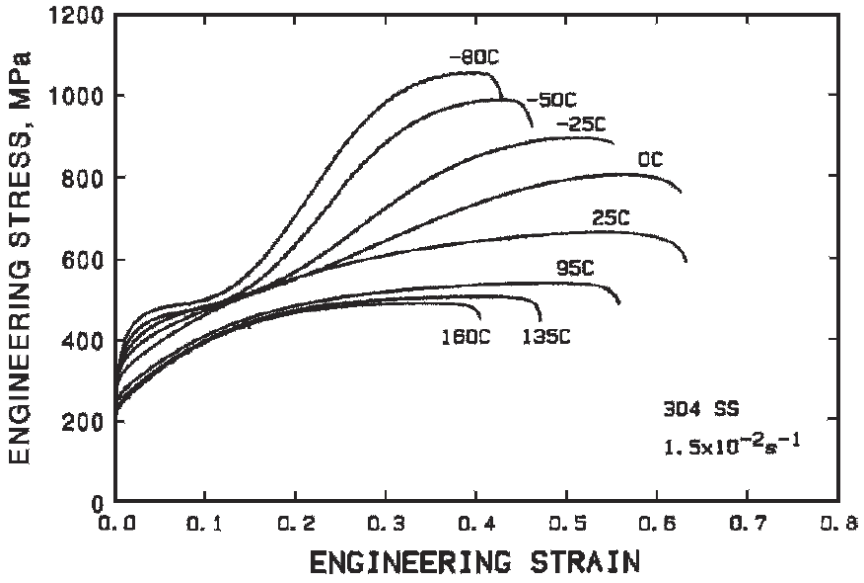

Fig 10 : Engineering stress-strain tensile data for type 304 stainless steel tested in the temperature range of –80 °C to 160 °C at an imposed engineering strain rate of 1.5 * 10^{-2} s^{-1} **[25].**

In the true stress-strain curve there is a change from a ‘‘parabolic’’ shape at room temperature to a sigmoidal or S-shape at lower test temperature **[25]**. The sigmoidal curve consists of an easy

deformation stage (plateau in the stress-strain curve at lower strains) followed by a rapid hardening stage at higher strains.

Gunter and Reed et al. [26] proposed that the easy deformation stage is due to ε martensite formation and the rapid hardening stage is due to α′-martensite formation, as ε-martensite tends to disappear at the beginning of the rapid hardening stage.

Tamura et al.[27] interpreted the first stage as being caused by the normal slip deformation mode plus deformation due to ε-martensite formation. Since ε-martensite formation stems from low stacking fault energy (SFE) of austenite, it is expected that deformation at low temperature will give rise to planar faults such as stacking faults, dislocation pile-ups, etc., and hence the formation of ε-martensite should manifest an increase in work hardening in the flow behavior.

Suzuki et al.[23] proposed from in situ electron microscopic observations of martensite formation in 18/8 stainless steel that the easy deformation stage is due to the formation of α′-martensite at the intersection of slip bands aided by the pile-up of dislocations. This proposition however, requires that α′-martensite can be the cause of both easy deformations in the first stage and rapid work hardening in the second stage.

It transpires from the aforesaid discussion that, for a better understanding of the plastic deformation behavior of austenitic stainless steels, it is a priori to have the knowledge on the martensitic transformation characteristics. Although quite an exhaustive number of research papers and journals exist for behavior under tensile testing conditions, but as per the knowledge of the current investigators no report is available for martensitic transformation and their quantification under compressive loading conditions.

Studies on martensitic deformation and compressive testing on various materials have started way back from 1950s.Among all these, a few important reports have been cited in **Table 1.**

Table 1: Some pertinent investigations related to tensile and compression tests of engineering materials as well as martensitic transformation of stainless steels.

Author	***Year***	***Material***	***Test***
Yao, Inui & Kishida	1994	Polysynthetically twinned crystals of Ti-Al	Tensile and compression testing
Jiang, Godfrey & Liu	2006	AZ31 magnesium alloy	Compression testing
Nijs, Holmedal & Fris	2006	Ultra fine grained Al-Mg alloy	Tensile and compression testing
Nave & Barnett	2004	Pure Magnesium	Parallel and perpendicular compression
Botshekan, Degallaix & Desplanques	1997	316 LN stainless steel	Tensile and low-cycle fatigue tests
Hashimoto & Byun	2008	316 stainless steel	Neutron irradiation tests
Smaga, Walther & Eifler	2006	AISI 304, AISI 321, AISI 348 stainless steels	Strain controlled fatigue tests
Biswas, Sivaprasad, Narasaiah & Tarafder	2006	304LN stainless steel	Load history effect on fatigue crack growth rate test
Bayerlein, Christ & Mughrabi	1988	AISI 304L stainless steel	Cyclic deformation at room temperature
Barnett, Keshavarz, Beer & Atwell	2004	Wrought Mg-3Al-1Zn	Compressive deformation

2.3. Solution Annealing of stainless steels

A solution annealing is a heat treatment operation that involves heating to around 960°C followed by quenching or rapid cooling which will restore the material to its original condition,

by removing alloy segregation, minimizing sensitization and restoring ductility after cold working. It takes the carbides that have precipitated in the grain boundaries and dissolves then into the surrounding matrix. Some alloys due to their low carbon content do not need a solution anneal due to carbide formation, but, benefit from a solution anneal to achieve maximum corrosion resistance **[28,29]**.

2.4. Compression testing at room temperature

The results of a simple compression test on a specimen of a ductile metal are virtually identical with those of a tensile test. A "simple compression test" is difficult to achieve, because of the friction that is necessarily present between the ends of the specimen and the pressure plates. Compression of the material causes an increase in area, and therefore a tendency to slide outward over the plates, against the shear stress on the interfaces due to the frictional resistance. Thus the state of stress cannot be one of simple compression. Lubrication of the interface helps the problem, as does the use of specimens that are reasonably slender — though not so slender as to cause buckling — so that, at least in the middle portion, a state of simple compressive stress is approached.

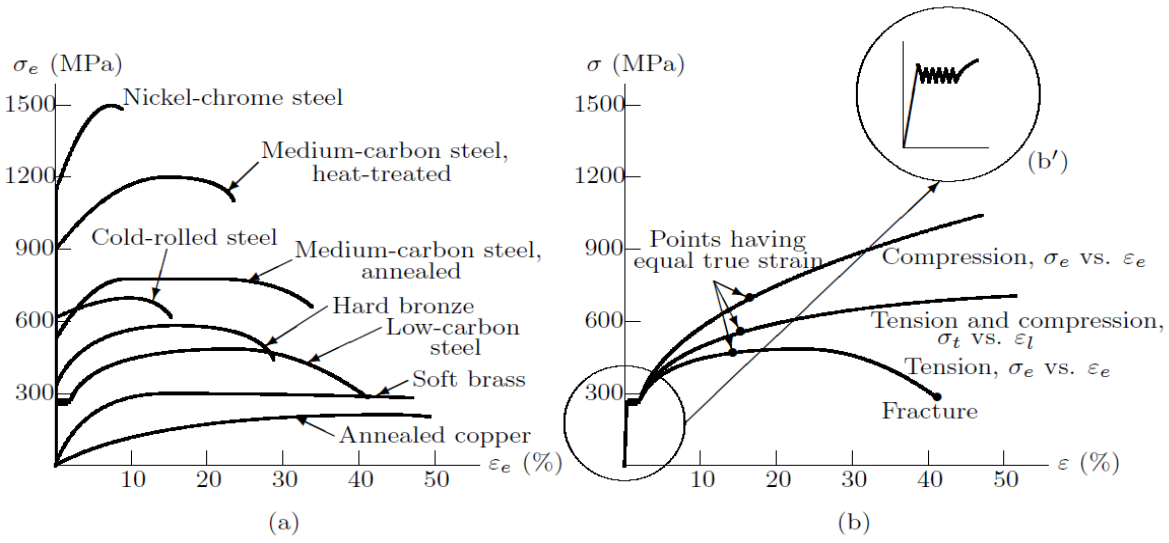

Figure continued to next page

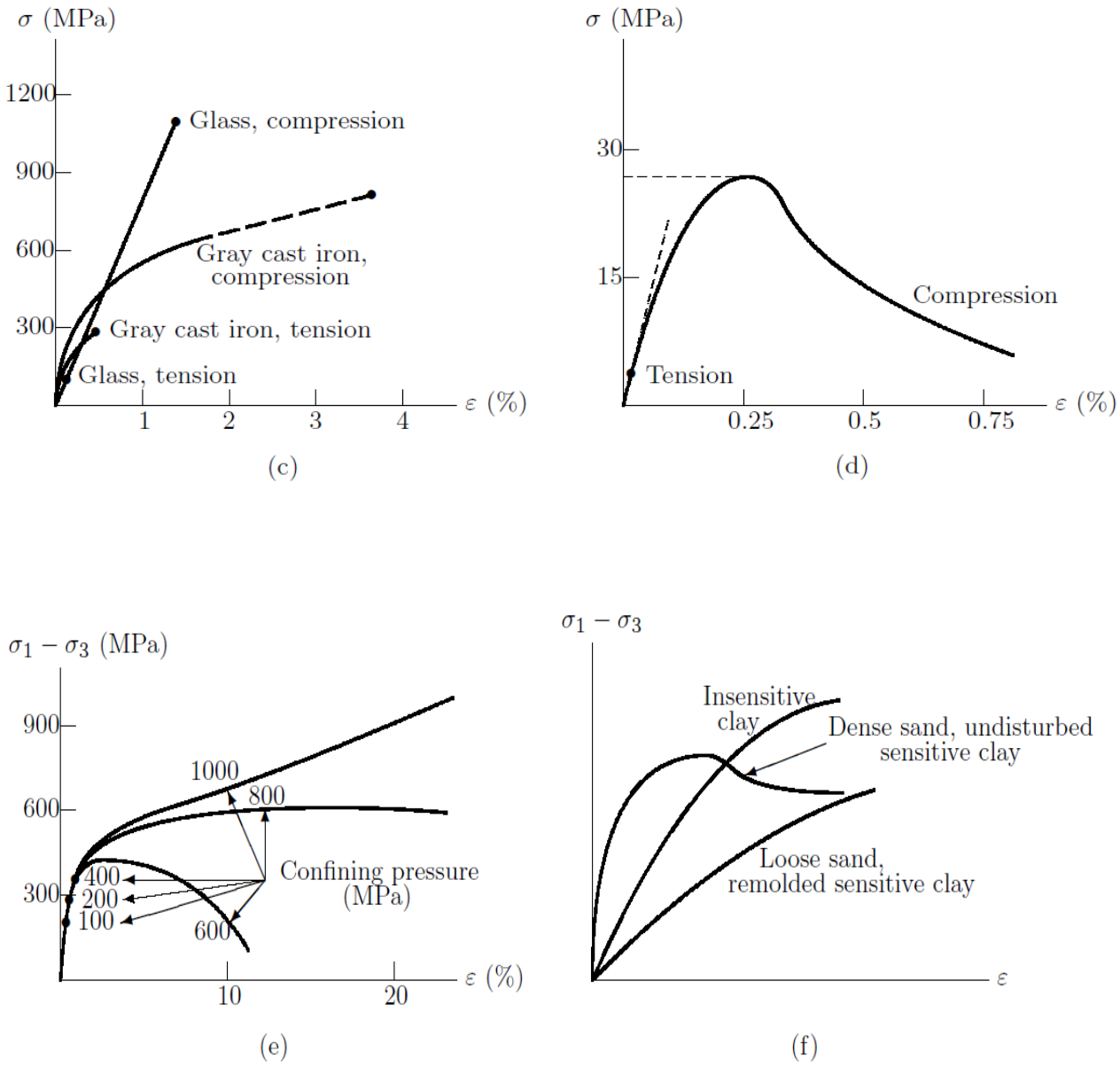

Fig 11: Stress-strain diagrams: (a) ductile metals, simple tension; (b) ductile metal (low carbon steel), simple tension and compression; (b') yield-point phenomenon; (c) cast iron and glass, simple compression and tension; (d) typical concrete or rock, simple compression and tension; (e) rock (limestone), triaxial compression; (f) soils, triaxial compression **[30]**.

Unlike ductile metals, brittle solids behave quite differently in tension and compression, the highest attainable stress in compression being many times that in tension. Classically brittle solids, such as cast iron or glass, fracture almost immediately after the proportional limit is attained, as in **Fig 11(c)**. Others, however, such as concrete and many rocks, produce stress-strain diagrams that are qualitatively similar to those of many ductile materials, as in **Fig 11(d)**. Of course, the strain scale is quite different: in brittle materials the largest strains attained rarely exceed 1%. The stress peak represents the onset of fracture, while the decrease in slope of the stress-strain curve represents a loss in stiffness due to progressive crack ing. The post-peak portion of the curve is highly sensitive to test conditions and specimen dimensions, and therefore it cannot be regarded as a material property. Moreover, it is not compression per se that brings about fracture, but the accompanying shear stresses and secondary tensile stresses.

The specimen in this test is in an axisymmetric, three-dimensional stress state, the principal stresses being the longitudinal stress σ_1 and the confining pressure $\sigma_2 = \sigma_3$, both taken conventionally as positive in compression, in contrast to the usual convention of solid mechanics. The results are usually plotted as $\sigma_1 - \sigma_3$ (which, when positive — as it usually is — equals $2\tau_{max}$) against the compressive longitudinal strain ε_1; typical curves are shown in **Fig 11(e) and (f) [30].**

2.5. Quantitative estimation of phase fractions

The quantitative estimation of phases by XRD can be done from total integrated intensity of all diffraction peaks for each phase. It is available in literature that integrated intensity is proportional to the volume fraction of the corresponding phase in a phase mixture. It can be stated that**[31]**:

$I_i^{hkl} = CR_i^{hkl}V_i/2\mu$ (1)

where,

$$C = \left(\frac{I_0 A\lambda^3}{32\pi r}\right)\left[\left(\frac{\mu_0}{4\pi}\right)\frac{e^4}{m^2}\right]$$ and,

$$R_{hkl} = \left(\frac{1}{\upsilon^2}\right)\left[|F|^2\ p\left(\frac{1+\cos^2 2\theta}{\sin^2\theta\cos\theta}\right)\right]\left(e^{-2M}\right)$$

In the mentioned equations, I_i^{hkl} : integrated intensity for (hkl) plane of i-phase, i: γ, α, or ε ;

C: the instrument factor;

R_i^{hkl} is the material scattering factor and depends on diffraction angle (θ), interplanar spacing of hkl, composition and crystal structure of phase i;

υ is the volume of unit cell,

F_{hkl} is the structure factor for reflecting phase (hkl),

The structure factor is independent of the shape and size of the unit cell.

p: multiplicity factor,

It can be defined as the number of different planes in a form having the same spacing. Parallel planes with different Miller indices, such as (100) and (-100), are counted separately as different planes, yielding numbers which are double those given in the preceding paragraph. Thus the multiplicity factor for the {100} planes of a cubic crystal is 6 and for the {111} planes 8.

e^{-2M} : temperature factor

The intensity of a diffracted beam decreases as the temperature is raised, and, for a constant temperature, thermal vibration causes a greater decrease in the reflected intensity at high angles than at low angles.

λ: the wavelength of incident X-ray beam,

μ: linear absorption coefficient,

A: cross sectional area of incident X-ray beam,

I_0 : intensity of the incident beam,

r: radius of diffractometer circle,

e, m: charge and mass of electron.

Therefore, for a steel containing austenite (γ), bcc martensite (α') and hcp-martensite (ε), then Eq. (1) may be written as:

$I_\gamma = K R_\gamma V_\gamma / 2\mu$,

$I_{\alpha'} = K R_{\alpha'} V_{\alpha'} / 2\mu$ and

$I_\varepsilon = K R_\varepsilon V_\varepsilon / 2\mu$.

Additionally,

$V\gamma + V\alpha' + V\varepsilon = 1$ (2)

From the above relations, and knowing that C/2μ is constant in a given X-ray diffraction scan, the volume fraction of austenite and martensite can be derived for numerous peaks as[2]:

$$V_i = \frac{\frac{1}{n}\sum_{j=1}^{n}\frac{I_i^j}{R_i^j}}{\frac{1}{n}\sum_{j=1}^{n}\frac{I_\gamma^j}{R_\gamma^j} + \frac{1}{n}\sum_{j=1}^{n}\frac{I_{\alpha'}^j}{R_{\alpha'}^j} + \frac{1}{n}\sum_{j=1}^{n}\frac{I_\varepsilon^j}{R_\varepsilon^j}} \quad (3)$$

where , i = γ, α' or ε in this instance and n is the number of peaks examined.

Eq. (3) enables simultaneous calculation of the volume fraction of austenite, α'-martensite and ε-martensite in 304L stainless steel from a single XRD scan.

Chapter 3

Experimental procedure

3.1 Introduction:

304L stainless steel were heat treated by a special heat treatment process called solution annealing. Samples of different dimensions (L/D) were cut for compression test. Tensile specimens are prepared. Composition of supplied steel was analysed with the help of an optical emission spectrometer. The samples of different L/D ratio were deformed by compression load. The microstructures of the undeformed samples and of deformed samples were observed under scanning electron microscope and by optical microscope. Phase transformation characteristic of different samples was studied by doing XRD. The hardness was measured with the Vickers hardness testing machine.

3.2 Material and heat treatment:

The available 304L grade austenitic stainless steel sample was in rod form. At first a few samples were cleaned to remove oils, grease and other types of residue; these were then allowed to undergo solution annealing, by heating at a temperature of 960°C for 1 hour followed by quenching in normal water. Water cooling is done to prevent sensitization i.e. to prevent precipitation of carbides at the grain boundaries.

3.3 Optical Emission Spectrometry:

The chemical compositions of 304L steel was evaluated using optical emission spectrometer (Model: ARL 3460 Metals Analyser, Thermo Electron Corporation Limited, Massachusetts, United States of America). The samples were cylindrical shape of 20 mm diameter and 10 mm height. Here, excitation is done by an arc or a spark and the analysis of the spectrum of frequencies of emitted electromagnetic radiation is done to identify the elements.

3.4 Tensile test:

Tensile deformations of the samples were done by using the universal testing machine (Model: INSTRON 8800, Instron Industrial Products, Pennsylvania, USA). Tensile tests were carried out with a crosshead speed of 1mm/min, which corresponds to nominal strain rate of 0.001 per second. During the tests, the load elongation data is captured by induced software, whose data is used for further analysis. The **figure 12** shows the dimensions for the specimen for this test. The numbers shown are the lengths in mm.

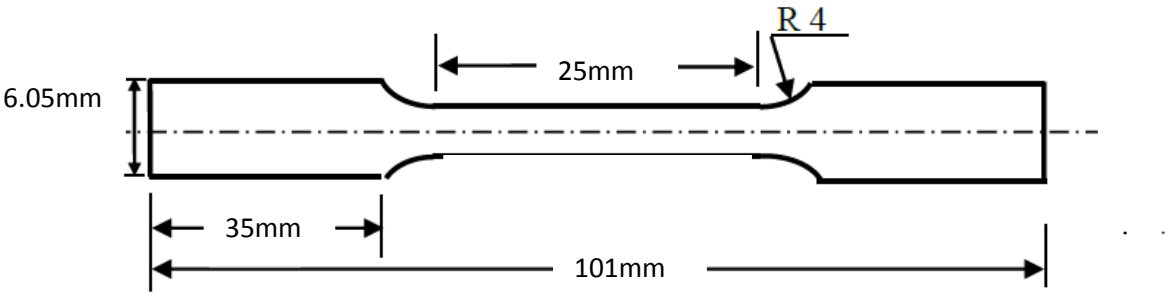

Fig 12: Tensile sample specification

Fig 13: Universal testing machine(tensile grip), INSTRON 8800

3.5 Compression test:

Samples of the investigated 304L stainless steel were deformed by applying compressive loads. The load is applied axially, uniformly and with negligible slip-stick friction.

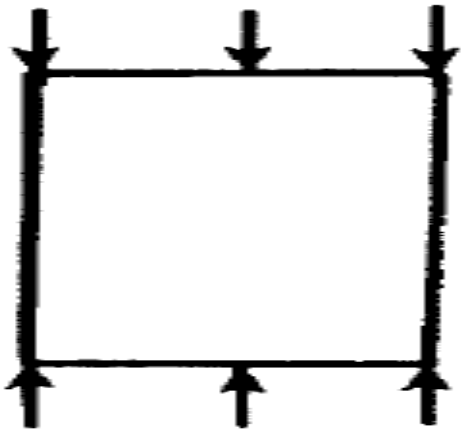

Fig 14: Direction of load application

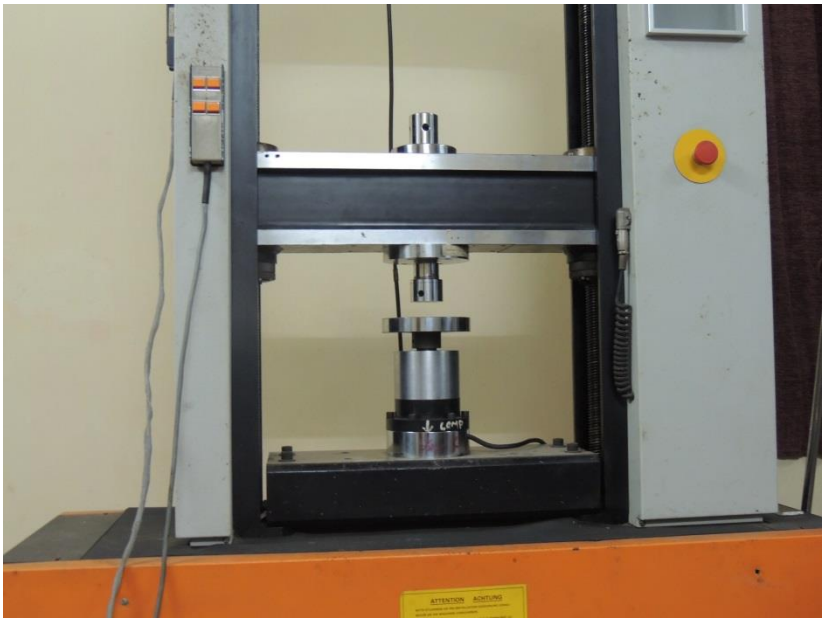

Fig 15: Universal testing machine (compression grip), INSTRON 1195

The heat treated samples were cut into cylindrical forms with different L/D ratios (**Table 2**) for performing compression tests.

Table 2: Compression test samples of different L/D ratios

Sl no.	Sample height (in mm)	Sample diameter (in mm)	L/D ratio
1	8	10	0.8
2	10	10	1.0
3	12	10	1.2
4	14	10	1.4
5	16	10	1.6

The samples were in cylindrical forms with maximum height of 16mm that was suitable for the test. The opposite surfaces of the samples were made parallel by polishing these up to 0.25 μm surface finish. To reduce the effects of friction, the specimen-platen interfaces were lubricated with TFE-fluorocarbon tape. The obtained data were used to plot the engineering curve for the investigated steel.

3.6 X-ray Diffraction:

The deformed samples were subjected for XRD analyses using Cu Kα radiation at 30 kV and 20 mA. The X-ray scan parameters used are as follows: scanning angle: 40 to 120 deg of 2θ; step size for scanning, 2 deg; time per step, 1 minute.

Fig 16: X-Ray Diffractometer

3.7 Scanning Electron Microscopy:

Microstructural characterization studies were done to observe the microstructure of undeformed sample surface and also the surface after deformation. This is done by using scanning electron microscope. The 304L stainless steel samples were mechanically polished using standard metallographic techniques before the examination. Characterization is done in etched conditions. Etching was done using the Aqua regia (3 volume part of hydro chloric acid (75%), 1volume part of Nitric acid(25%)). The SEM micrographs of the samples were obtained. The images were taken in secondary electron (SE) mode. This analysis was done by a scanning electron microscope equipped with Energy Dispersive X-Ray Spectroscopy (EDS) (Model: JEOL 6480 LV scanning electron microscope, JEOL Limited, Japan).

Fig 17:JEOL JSM-6480LV scanning electron microscope

3.8 Optical Microscopy:

Microstructures of the compression samples were observed under computerized optical microscope (Model: Olympus BX51, Essex, UK). The stainless steel samples of different L/D ratio were mechanically polished using standard metallographic techniques before the examination. Characterization is done in etched conditions. Etching was done using the Aqua regia (3 volume part of hydro chloric acid (75%), 1volume part of Nitric acid(25%)). The micrographs of the samples were obtained.

Fig 18: Computerized Optical Microscope

3.9 Vickers Hardness Test

The macro hardness tests of all the samples have been done using a Vicker's hardness testing machine. The applied load during the testing was 20 kgf, with a dwell time of 10 s. It has a square-base diamond pyramid indenter. The Vickers hardness number (VHN) is calculated from the following equation:

$$VHN = \frac{1.854\,P}{D^2}$$

where P = applied load, kgf

D = average length of diagonals, mm

Fig 19: Vickers hardness testing machine

Chapter 4

Results and discussion

4.1 Introduction:

Different tests like compositional analyses, tensile testss, compression test, XRD,SEM etc. were carried out on the 304L stainless steel samples. The results obtained from these tests are reported, analyzed and discussed further in this chapter.

4.2 Compositional Analysis:

The following table shows the weight percentage of different elements present in the supplied 304L stainless steel sample.

Table 3: Compositional analyses of the investigated 304L stainless steel.

Element	Wt. %
C	0.03
S	0.016
P	0.042
Si	0.533
V	0.068
Al	0.035
Ti	0.019
Cr	18.2
Mo	0.2
Cu	1.05
Ni	7.9
Fe	Balance

The weight percentage of chromium and nickel were found to be 18.2% and 7.9%, which is very close to 18% and 8% respectively. This suggests that the provided sample is 304L austenitic stainless steel. And the C% of 0.03%, results in minimization of sensitization and further does not demand post-welding treatments.

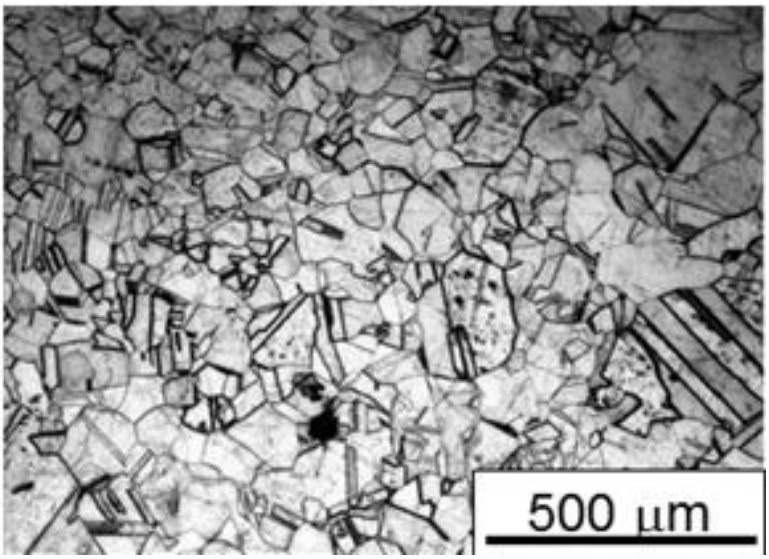

Fig. 20: Microstructure of the undeformed 304L stainless steel sample

The optical microstructure of the investigated AISI 304Lstainless steel is illustrated in **Fig. 20.** Typical austenitic grains can be observed from this figure along with presence of annealing twins at a few places. The grain size is measured using linear intercept method and was found to be 55.73±3.81µm. The smaller magnitude of standard deviation indicates that the steel is having almost uniform distribution of the grains.

4.3 Results of compression test:

Figure 21 shows the engineering stress-strain relationship obtained after performing the compression tests for the 304L stainless steel samples of different L/D ratios. The applied load in the test was restricted to 98kN. It is evident from the plots that the deformation is homogenous up to about 15% strain for all the specimens after which the lubrication has gradually lost its effect. So friction has prevailed at the specimen-platen interfaces that have added to increase in strength values. The percentage deformation achieved varies from specimen to specimen and the values of maximum strain percentage obtained have been reported in **Table 4.**

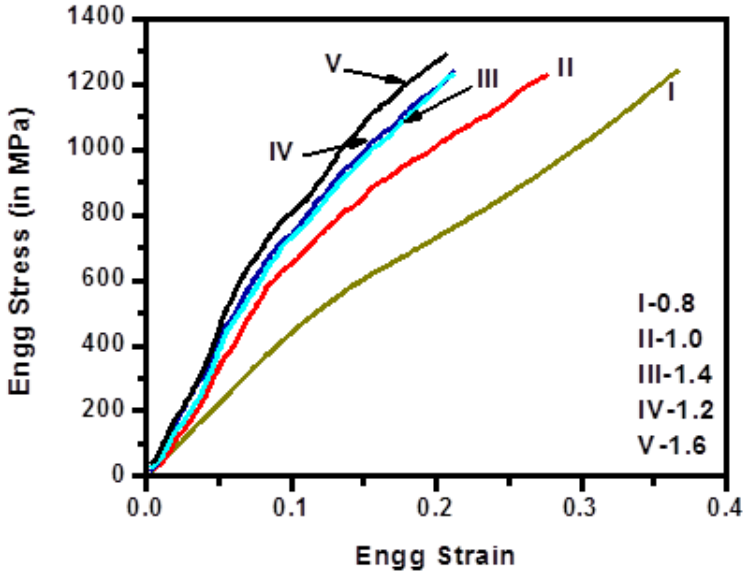

Fig 21: Engineering stress-strain plots for 304L stainless steel compressed to 98kN load. Values with the curves indicate different L/D ratios.

Table 4: Maximum deformation values obtained for compression tested samples

Sl. No.	L/D ratio	Deformation (Strain %)
1	0.8	34.0
2	1.0	33.0
3	1.2	28.5
4	1.4	27.5
5	1.6	24.5

From the values obtained in **Table 4,** it can clearly be stated that as the length increases, keeping the diameter constant, then deformation obtained will decrease, under the same loading condition.

The yield strength value has been calculated by offset method (offset =0.2%) as specified in ASTM standard E9 and it was found to be around 350 MPa for all samples.

4.4 Strain-hardening exponent and strength coefficient:

If the stress and strain measurements are based on instantaneous measurements, then the curve obtained is known as a true stress-strain curve or a flow curve as it will represent the plastic flow characteristics of the material.

The true stress σ is expressed in terms of engineering stress s by $\sigma = s\,(1+e)$

The true strain is determined from conventional strain ε by $\varepsilon = \ln(1+e)$

The flow curve in the region of uniform plastic deformation can be expressed by the simple power curve relation given as:

$\sigma = K\,\varepsilon^{n}$, where n is the strain-hardening exponent and K is the strength coefficient.

A log-log plot of true stress and true strain up to maximum load will result in a straight line. The linear slope of this line is n and K is the true stress at ε = 1.0.

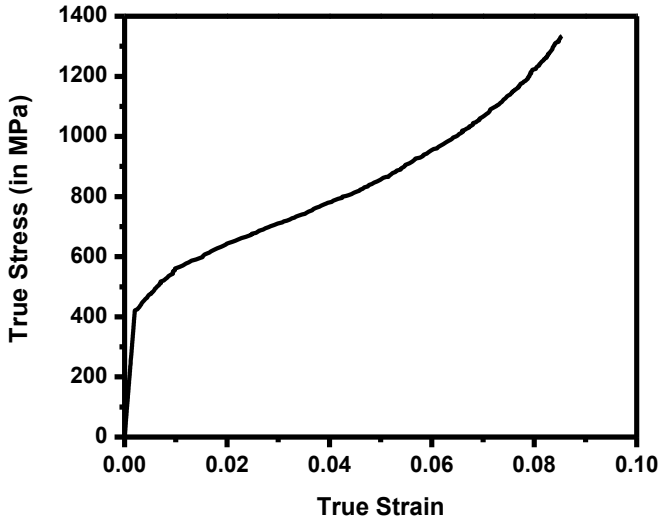

Fig 22: True stress strain plot for the sample with L/D =1.0 compressed to 98kN.

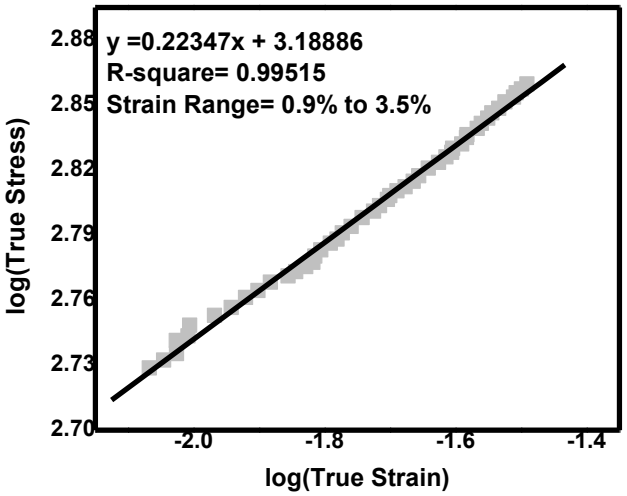

Fig 23: Linear part of the plastic region of the log-log plot for the sample with L/D = 1.0 compressed to 98kN.

From the above figure it can be stated that the strain hardening exponent is around 0.223 and the strength coefficient is 1545 MPa.

In the similar fashion the true stress strain plots were done for the remaining samples, the plots of which have been merged together as shown below in **figure 25**.

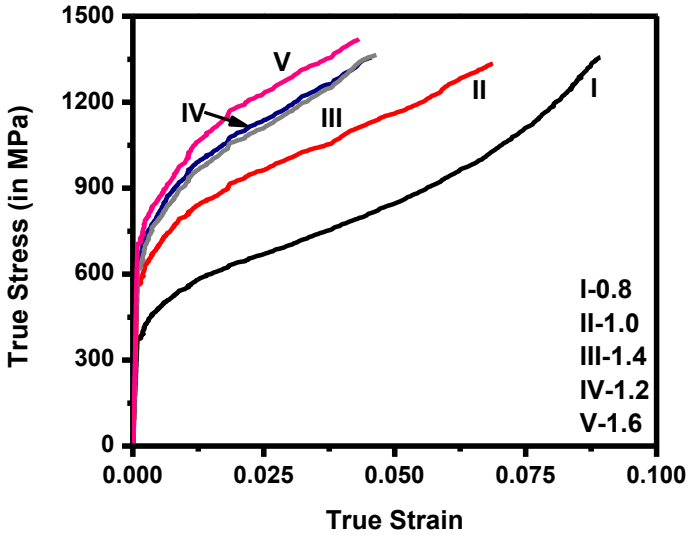

Fig 24: True stress strain plots for the other investigated samples compressed to 98 kN. The values indicate the different L/D ratios.

The strain hardening coefficients and the strength coefficients were determined for the remaining samples and the values are summarized in the table below:

Table 5: n and K values for samples compressed to 98kN with varying L/D ratios.

L/D ratio	Strain hardening exponent (n)	Strength Coefficient (K,MPa)
0.8	0.201	1400
1.0	0.223	1545
1.2	0.257	1670
1.4	0.210	1356
1.6	0.208	1630

Similar calculations were also performed for sample that was tensile tested with 2% strain rate up to failure.

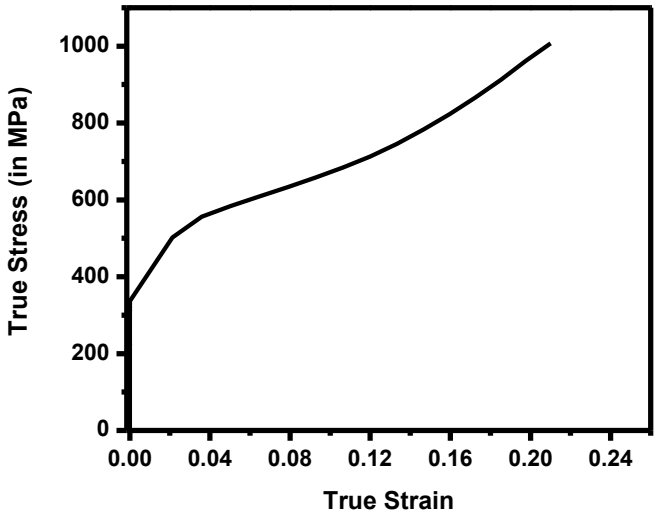

Fig 25: True stress-strain plot for 304L stainless steel sample with 2% strain rate

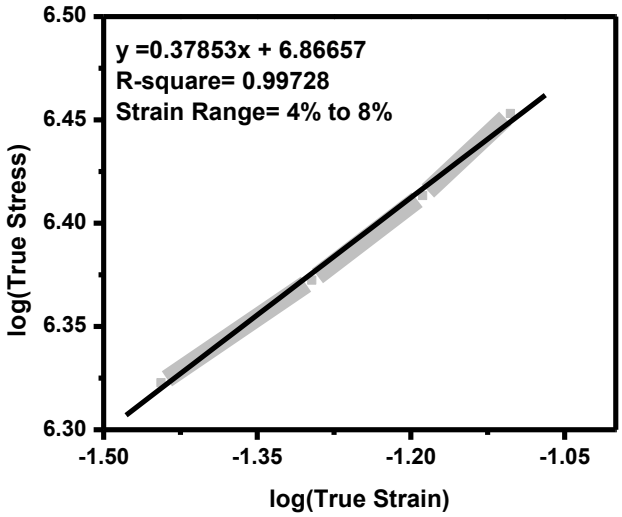

Fig 26: Linear part of the plastic region of the log-log plot for the above sample

Here the strain hardening coefficient was found to be 0.38 in the strain range of 4%-8% used.

4.5 Microstructural analysis:

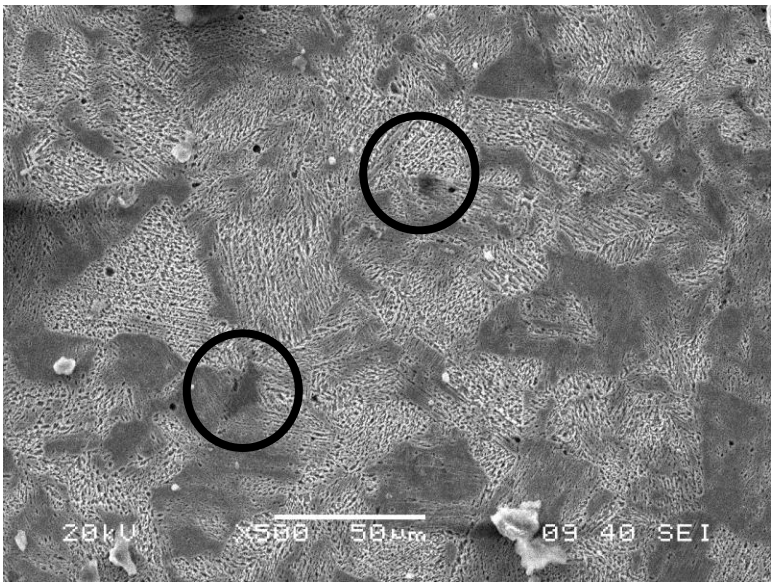

Fig. 27(a): Microstructure of the deformed 304L stainless steel tensile sample at 2% strain rate

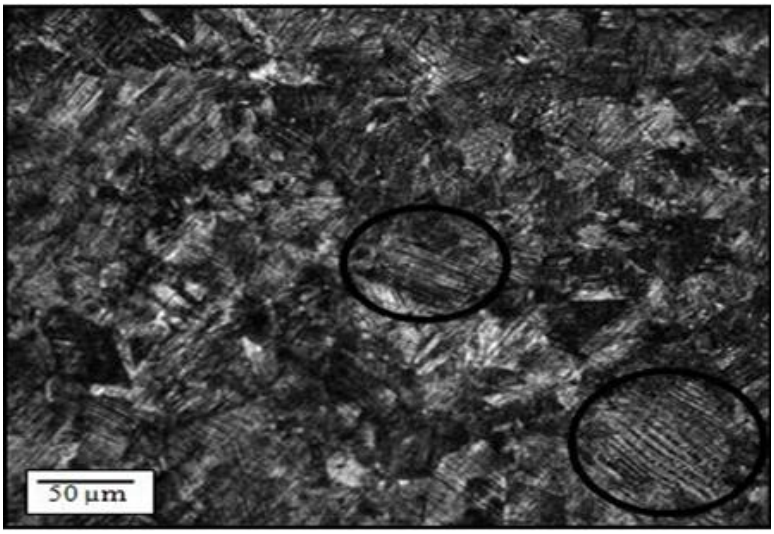

Fig 27(b): Microstructure of the deformed 304L stainless steel sample compressed to 98kN with L/D =1.2

The highlighted portions in **Fig. 27(a), 27(b)** show for possibility of transformation induced martensite. In comparison to **Fig. 20**, there are no such martensitic regions, which is a clear indication that considerable transformation has taken place due to tensile and compressive loading.

4.6 Hardness values:

Table 6: Comparison of hardness values of various test samples

Sample	***Vickers macro-hardness (20kg load) (VHN)***	
Undeformed	205±4.6	
Deformed by compression	L/D=0.8	441
	L/D=1.0	405
	L/D=1.2	401
	L/D=1.4	395
	L/D=1.6	395
Deformed by tension	506	

From the above table it is evident that deformation significantly increases the hardness values of the investigated sample. From the compression test results, it can be stated that the hardness values decrease on increasing the L/D ratios. The increases in hardness values on deformation are due to the possibility of formation of transformation induced martensite.

4.7 Quantitative phase analyses from XRD results:

Typical XRD plots of undeformed and deformed specimens are shown in **Fig. 28**. The diffraction scan was obtained at room temperature using Cu Kα radiation with scanning angle being varied between 40^0 to 120^0.

It can be observed from **Fig. 28** that only austenite peaks are present in the XRD profile.

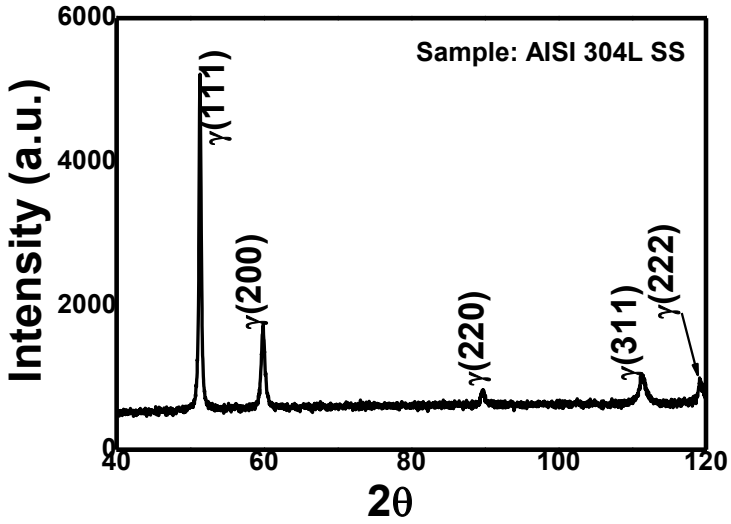

Fig. 28: XRD profile of the undeformed 304L stainless steel sample

Using the same scanning range and step size, the XRD analyses were also carried out for the different 304L stainless steel samples with varying L/D ratios.

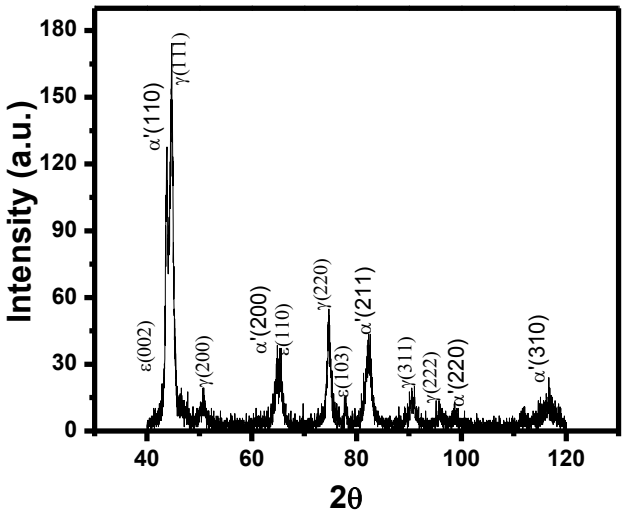

Fig. 29(a): XRD profile of the deformed 304L stainless steel sample with L/D = 0.8

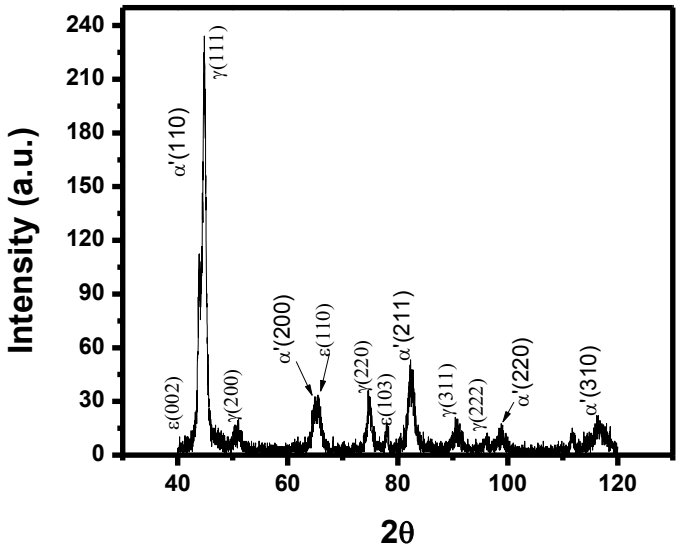

Fig. 29(b): XRD profile of the deformed 304L stainless steel sample with L/D = 1.2

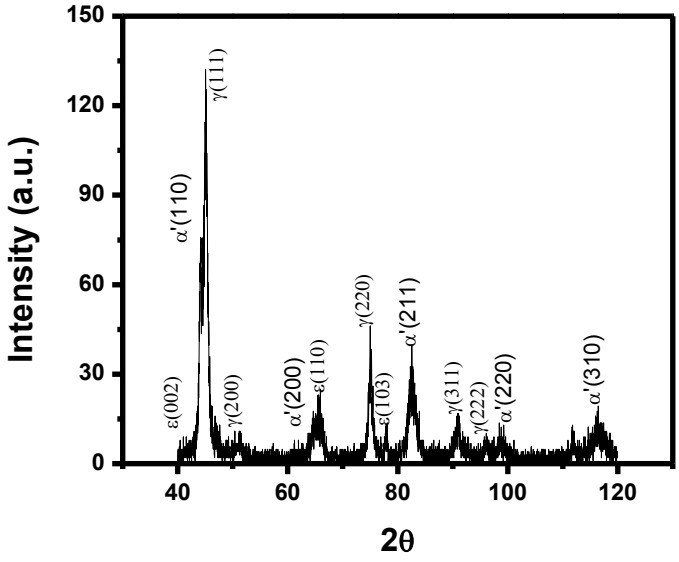

Fig. 29(c): XRD profile of the deformed 304L stainless steel sample with L/D = 1.6

A few numbers of α'- and ε-martensite peaks are present in the deformed 304L stainless steel samples that have been compressed to 98kN load with different L/D ratios. The individual

diffracting planes from the fcc austenite, hcp-martensite and bcc martensite can be clearly identified and are shown in **Fig. 29.**

The different XRD plots the compressed 304L stainless steel samples with different L/D ratios can be merged together to be shown in the **figure 30** below.

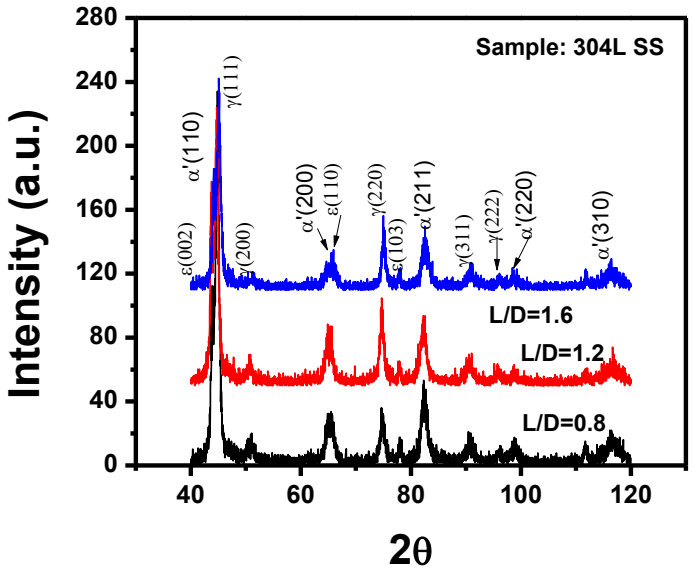

Fig. 30: XRD profile of the deformed 304L stainless steel samples with L/D ratios of 0.8, 1.2 and 1.6 showing different peaks.

The presence of $(002)_{\varepsilon}$, $(110)_{\varepsilon}$ and $(103)_{\varepsilon}$ peaks are clearly revealed and indicate the formation of the hexagonal ε–martensite phase during deformation. Additionally the $(110)_{\alpha'}$, $(200)_{\alpha'}$, $(211)_{\alpha'}$, $(220)_{\alpha'}$ and $(310)_{\alpha'}$ peaks are present characterizing the bcc-martensite.

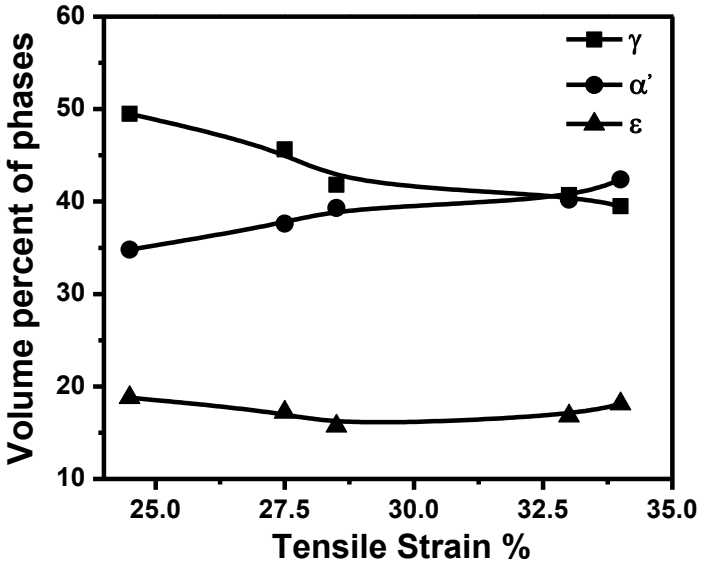

Fig. 31: Variation in martensite and retained austenite phase fractions as a function of strain .

The volume fraction of austenite, ε-martensite and α'-martensite phases as a result of deformation process have been calculated using **Eq. (3)** as a function of strain. At a closer look, on **Fig. 5**, it can be stated that as the strain percent increases, proportion of α'- martensite gradually increases. However ε-martensite being an intermediate phase in the transformation process has an almost constant volume fraction throughout the strain range used **[32]**.

Das et al. [20] have examined the effect of tensile loading on 304LN stainless steel in terms of variation of volume fraction of martensite formed as a function of true strain that has been shown in **Fig. 8**. A nucleated α′-martensite at the intersection of two shear bands has been shown in **figure 32**. The embryo shown in **figure 32** is a commonly known α′-martensite formation site in austenitic stainless steels and is referred as strain induced martensite.

De et al. [3] summarizes the volume fraction of austenite, □ and □′-martensite phases as a function of deformation strain at -50^0 C under tensile loading for two different grain sizes of the 304L stainless steel that has been shown in **figure 33**.

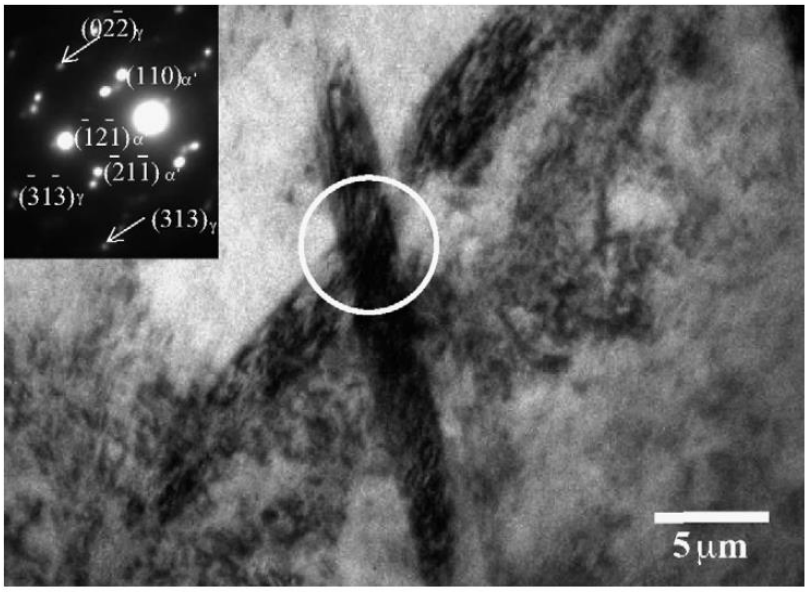

Fig. 32: Formation of α′-martensite (bcc) with zone axis of [−113] in γ-austenite (fcc) with zone axis of [−2 3 3] at the micro-shear band intersection (at strain rate of 1.0 s−1) **[20]**.

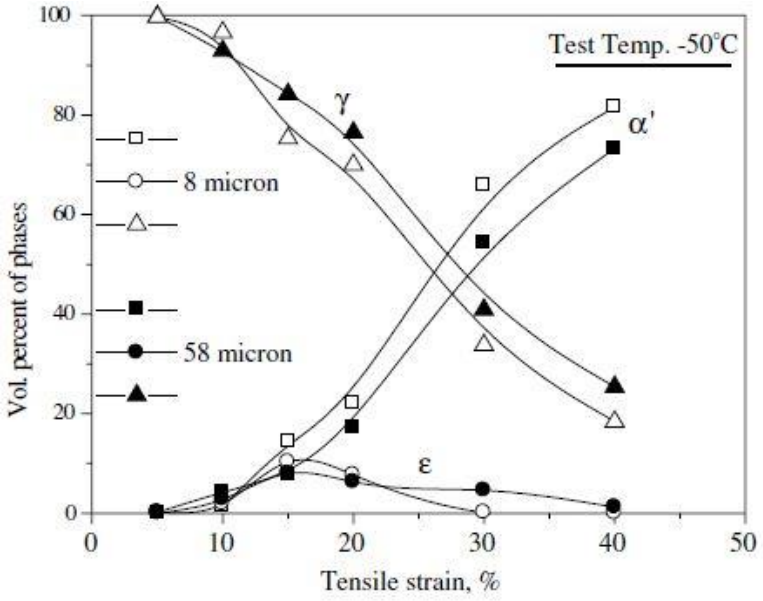

Fig. 33: Variation in martensite & retained austenite phase fraction as a function of strain at -50^{0}C **[3]**.

The present obtained results have shown similar extent of transformation can take place up on compressive loading.

Chapter 5

Conclusions

Conclusions

The primary aim of the work was to study the compression behavior of 304L stainless steel and associated variation in the microstructure of the steel by the formation of martensitic phase. From the results and their pertinent analyses lead to infer the following conclusions:

- It has been found that deformation is usually homogenous up to 15% strain for all the specimens having various lengths to diameter ratios. The effect of lubrication loses and friction plays a significant role in increasing strength values after the aforesaid strain value.
- Compressive deformation induces martensite (both α' and ε- martensite) formation in the investigated steel which is confirmed by using the results of X-ray diffraction (XRD) plots.
- Further, the quantitative method used in calculating volume fractions as a result of deformation reveals an increase in α' phase fraction with increase in percentage deformation and that of ε-martensite phase fraction remains almost constant over the strain range used.

The future prospect would be to use molybdenum silicide at the specimen platen interfaces and study its effect in reducing the effects of friction. Further compression test on stainless steel can be carried out using varying strain rates and at different test temperatures so as to compare its behavior as-against tensile loading conditions.

References

[1] W. S. Lee, C. F. Lin: Scripta Mater (2000), 43, 777-82.

[2] Stainless Steels for design Engineers (# 05231G) 2008 , ASM International, Ch-6, Austenitic stainless steels.

[3] A. K. De, D. C. Murdock, M. C. Mataya, J. G. Speer, D. K. Matlock: Scripta Mater (2004), 50, pp 1445–49.

[4] L Mangonon, G. Thomas: Metall. Trans., (1970), 1587-90.

[5] en.wikipedia.org/wiki/Stainless_steel (as on 05.05.2013)

[6] H.Nordberg, Mechanical properties of Austenitic and Duplex Stainless Steels. Florens, 1993.

[7] D Peckner, I M Bernstein, Handbook of Stainless Steels, McGraw-Hill, 1977,pp 282.

[8] Corrosion Resistance of the Austenite Chromium-Nickel Stainless Steels in High Temperature environments, International Nickel Assosciation Berlin, 1985,pp 145.

[9] www.sppusa.com/Stainless_Steel_Products (as on 05.05.2013)

[10] T. Angel: J. Iron Steel Inst., 1954, vol. 177, pp. 165-74.

[11] B. Cina: J. Iron Steel Inst., 1954, vol. 177, pp. 406-22.

[12] V. Shrinivas, S.K. Varma, and L.E. Murr: Metall. Mater. Trans. A,1995, vol. 26A (3), pp. 661-71.

[13] Ha, T.K., & Chang, Y.W. Acta Mater, (1998), 46(8), pp 2741-45.

[14] Ha, T.K., Sung, H.J., Kim, K.S.& Chang, Y.W. (1999). Met Sci Eng A (271),pp 160-68.

[15] A.L. Schaeffler, Met. Prog. Databook 6 (1973),pp 207-10.

[16] U. Krupp, C. West, H-J. Christ, Mater. Sci. Eng.A(2007), pp. 1016-21.

[17] H.J. Maier, B. Donath, M. Bayerlein, H. Mughrabi, B. Meier, M. Kesten, Z. Metallkd, Metall. Mater. Trans. A(84), (1993),pp 12-21.

[18] K. Dutta, S. Sivaprasad, S. Tarafder, K.K. Ray, Materials Science and Engineering A (527) 2010, pp 7571–79

[19] J. Talonen, H. Hanninen, Acta Mater. 55 (2007),pp 6108–18.

[20] A Das, S. Sivaprasad, M. Ghosh, P. C. Chakraborti, S. Tarafder: Mater. Sci. Eng. A (2007) 486 (1-2),pp. 283-86.

[21] J.F. Breedis and W.D. Robertson: Acta Metall., 1962, vol. 10, pp.1077-88.

[22] P.L. Mangonon, Jr. and G. Thomas: Metall. Trans. A, 1970, vol. 1A (6), pp. 1577-86.

[23] T. Suzuki, H. Kojima, K. Suzuki, T. Hashimoto, and M. Ichihara: Acta Metall., 1977, vol. 25, pp. 1151-62.

[24] J.W. Brooks, M.H. Loretto, and R.E. Smallman: Acta Metall., 1979, vol. 27, pp. 1829-38.

[25] G.L. Huang, D.K. Matlock, and G. Krauss: Metall. Trans. A, 1989, vol. 20A, pp. 1239-46.

[26] C.J. Guntner and R.P. Reed: Trans. ASM, 1962, vol. 55, pp. 399-419.

[27] I. Tamura, T. Maki, and H. Hato: Trans. ISIJ, 1970, vol. 10 (3), pp. 163-72.

[28] http://www.thermtech.net/castings/solution-annealing-stainless-steels (as on 05.05.2013)

[29]http://www.thermalfurnaces.com/solution_annealing_furnace_for_stainless_steel_wirerods (as on 05.05.2013)

[30] www.ce.berkeley.edu/plas/CH-2 (as on 05.05.2013)

[31] B. D. Cullity, S. R. Stock, Elements of X-Ray Diffraction, 3rd ed. New Jersey,2001,pp 351.

[32] J. Talonen, N. Pertti, P.Gersom, H.Hanninen, Metall. Trans. A (2005), 36, pp 421–32.